A Density Functional Theory Investigation on the Mechanism and Kinetics of Dimethyl Carbonate Formation on Cu_2O Catalyst

Riguang Zhang,[a] Luzhi Song,[a] Baojun Wang,*[a] and Zhong Li[a]

A theoretical analysis about the mechanism and kinetics of dimethyl carbonate (DMC) formation via oxidative carbonylation of methanol on Cu_2O catalyst is explored using periodic density functional calculations, both in gas phase and in solvent. The effect of solvent is taken into account using the conductor-like screening model. The calculated results show that CO insertion to methoxide species to produce monomethyl carbonate species is the rate-determining step, the corresponding activation barrier is 161.9 kJ mol^{-1}. Then, monomethyl carbonate species reacts with additional methoxide to form DMC with an activation barrier of 98.8 kJ mol^{-1}, above reaction pathway mainly contributes to the formation of DMC. CO insertion to dimethoxide species to form DMC is also considered and analyzed, the corresponding activation barrier is 308.5 kJ mol^{-1}, suggesting that CO insertion to dimethoxide species is not competitive in dynamics in comparison with CO insertion to methoxide species. The solvent effects on CO insertion to methoxide species involving the activation barriers suggest that the rate-determining step can be significantly affected by the solvent, 70.2 kJ mol^{-1} in methanol and 63.9 kJ mol^{-1} in water, which means that solvent effect can reduce the activation barrier of CO insertion to methoxide species and make the reaction of CO insertion to methoxide in solvents much easier than that in gas phase. Above calculated results can provide good theoretical guidance for the mechanism and kinetics of DMC formation and suggest that solvent effect can well improve the performance of DMC formation on Cu_2O catalyst in a liquid-phase slurry. © 2012 Wiley Periodicals, Inc.

DOI: 10.1002/jcc.22939

Introduction

Many researchers have been drawing attention to dimethyl carbonate (DMC) due to its use in replacing environmentally unfriendly compounds.[1,2] The oxidative carbonylation of methanol has been pursued over a variety of copper catalysts as an "environment friendly," nonphosgene production pathway to DMC,[3–19] in which two methods including gas phase[11–16] and liquid-phase method[17–19] are involved.

It is well known that Cu^+ ions have been postulated to be the active species for DMC formation by the oxidative carbonylation of methanol.[6,16] So CuCl has been widely used as the active component,[6,17,18] but there are several problems such as the equipment corrosion and the catalyst deactivation due to Cl^- loss. To avoid these problems, several authors have examined the potential of copper-exchanged zeolites as catalysts,[6,12–14] and researches by King[8] have shown that Cu—Y zeolite exhibited good activity and selectivity for DMC formation with little catalyst deactivation. Moreover, King et al.[5] have discovered that chloride was not necessary for copper to catalyze the oxidative carbonylation of methanol. Thus, Cu_2O has been chosen as a chlorine-free and ideal model system to investigate the catalytic mechanism for the oxidative carbonylation of methanol to DMC. For example, Wang et al.[20] reported a new type of supported oxide catalyst CuO—La_2O_3/activate carbon (AC), which contained CuO and Cu_2O simultaneously providing Cu^{II} and Cu^{I}. King[21] prepared the chlorine-free Cu_2O/LZ-20M catalyst by heating a mixture of Cu_2O with HY zeolite at 650°C, which showed a high catalytic activity. Recently, our group[22] have prepared the chlorine-free catalyst Cu_2O/AC by dipping $Cu(CH_3COO)_2$ onto AC surface, the Cu_2O/AC catalyst performs a good catalytic activity for the oxidative carbonylation of methanol, in which Cu_2O has been postulated to be the catalytic active species. Further, the treatment of AC with ammonia is in favor of Cu_2O dispersion and can well improve the catalytic activity and selecivity.[23]

A large number of experimental studies about the mechanism and kinetics of DMC formation over CuCl catalyst[3] or Cu-exchanged zeolites have been reported.[6,8,12,13,16,21,24] In these studies, two different pathways for DMC formation are proposed, one is the pathway involving CH_3OH dehydration to form the dimethoxide species $(CH_3O)_2$; subsequently, CO insertion to $(CH_3O)_2$ to produce DMC. The other is the pathway involving CO insertion to methoxide species to form CH_3OCO; once formed, CH_3OCO reacts rapidly with another CH_3O to form DMC. CO insertion to methoxide species or dimethoxide species is proposed to be the rate-determining step. However, the $(CH_3O)_2$ cannot be discerned experimentally because the vibrational spectra of CH_3O group in$(CH_3O)_2$ and in CH_3O are virtually

[a] R. Zhang, L. Song, B. Wang, Z. Li
Key Laboratory of Coal Science and Technology of Ministry of Education and Shanxi Province, Taiyuan University of Technology, Taiyuan 030024, Shanxi, People's Republic of China Fax: (+86) 351 6041237
E-mail: wangbaojun@tyut.edu.cn

Contract/grant sponsor: National Natural Science Foundation of China; Contract/grant number: 20906066; Grant number: 20976115.

the same. So the experiments cannot obtain the detailed reaction mechanism, which mainly contributes to DMC formation in these two reaction pathways proposed. In addition, in a liquid-phase slurry, a detailed understanding about solvent effect on the mechanism and kinetics of DMC formation under the reaction environment of liquid-phase slurry is seldom considered. However, many researches have shown that the chemical characteristic and reaction barrier in liquid-phase environment are different from those in gas phase, namely, the reaction environments might change the chemical characteristic and reaction barrier, in which the solvent environment plays an important role.[25–36] Therefore, it is of great significance to study the detailed mechanism and kinetics of DMC formation both in gas phase and in liquid-phase environment.

Nowadays, experimental information is not always sufficient and accompanying theoretical calculations can be helpful to clarify some questions. Computational chemistry methodologies have been used as a powerful tool to study the mechanism and kinetics of several chemical reactions.[37] By means of theoretical calculation, it may be possible to better understand the mechanism and the kinetics of DMC formation. Up to now, to our knowledge, few theoretical studies for the mechanism and kinetics of DMC formation are reported. Only Bell and coworker[38] reported the mechanism of DMC formation via oxidative carbonylation of methanol in gas phase on Cu—Y zeolite using density functional theory (DFT) method, in which single atom Cu^+ cation was located to represent the catalytically active site. However, single atom cluster cannot model and reflect a specific crystal plane.[39]

$Cu_2O(111)$ has been proved to be the main surface of Cu_2O by X-ray diffraction characterization (XRD).[40,41] Therefore, in this study, we carry out a detailed investigation about the mechanism and kinetics of DMC formation on $Cu_2O(111)$ surface both in gas phase and in liquid-phase environment using periodic density functional calculations, which can well avoid the well-known boundary effects associated with cluster model calculations. The following two questions by means of first-principle calculation wish to be solved at the microscopic level: (a) in the reported two pathways of DMC formation, which is the main pathway contributing to DMC formation? (b) What role does the solvent environment of the liquid-phase slurry play in the mechanism and kinetics of DMC formation? Our results are expected to understand the detailed mechanism and kinetics of DMC formation on Cu_2O catalyst as well as the solvent effect on the reaction kinetics. In addition, although the chemical environment of Cu^+ ions in Cu_2O differs from that of Cu^+ ions in copper-exchanged zeolites, we expect that the calculated results about the mechanism and kinetics of DMC formation over Cu_2O catalyst may contribute to understanding that in other chlorine-free catalyst.

Computational Model and Method

Surface model

$Cu_2O(111)$ surface is modeled by using the supercell approach, where periodic boundary condition is applied to the central supercell so that it is reproduced periodically throughout space. The ideal and perfect $Cu_2O(111)$ surface is nonpolar including four chemically different types of surface atoms, which are denoted as Cu_{CUS}, Cu_{CSA}, O_{SUF}, and O_{SUB} shown in Figure 1. Cu_{CUS} is the surface copper that is coordinatively unsaturated, that is, singly coordinated Cu^+ cation. Cu_{CSA} is the coordinatively saturated copper atom, that is, doubly coordinated Cu^+. O_{SUF} is the outer-most surface oxygen, that is, threefold-coordinated oxygen anions. O_{SUB} is the subsurface oxygen, that is, fourfold-coordinated oxygen anion. A [2 × 2] supercell with six atomic layers is used as substrate, as shown in Figure 1. In the computation, the substrate is kept fixed to the bulk coordinates; the reason of keeping substrate frozen has been explained in our previous paper.[42] The adsorbates are allowed to relax in all of the geometry optimization calculations, the vacuum space of 1.0 nm is inserted in the direction perpendicular to the surface, at such a distance there is little interaction between the neighboring layers.

Computational method

DFT has been used to perform for all calculations using the generalized gradient approximation (GGA) with the Becke–Lee–Yang–Parr exchange-correlation functional. In the computation, the inner electrons of copper atoms are kept frozen and replaced by an effective core potential, other atoms are treated with an all electron basis set. The double-numeric basis with polarization functions is used for all atoms in the adsorbed and substrate systems. The *k*-point sampling scheme of Monkhorst–Pack grid of 4 × 4 × 1 and Methfessel–Paxton smearing of 0.005 Hartree are used. All calculations are carried out with the $Dmol^3$ program package in Materials Studio 4.4[43,44] on HP Proliant DL 380 G5 server system.

In this work, the liquid-phase environment is described by solvent effect using the conductor-like screening model (COSMO) implemented into $Dmol^3$.[45,46] COSMO is a continuum solvation model where the solute molecule forms a cavity within the dielectric continuum of permittivity, ε that represents the solvent.[47,48] The charge distribution of solute polarizes the dielectric medium. The response of dielectric medium is described by the generation of screening (or polarization) charges on the cavity surface. COSMO does not require the solution of the rather complicated boundary conditions for a dielectric to obtain screening charges but instead calculates the screening charges by using a much simpler boundary condition for a conductor. These charges are then scaled by a factor $f(\varepsilon) = (\varepsilon - 1)/(\varepsilon + 0.5)$, to obtain a rather good approximation for the screening charges in a dielectric medium. In this study, based on the reaction environments for DMC formation by the oxidative carbonylation of methanol in a liquid-phase slurry, values of solvent dielectric constants $\varepsilon = 32.63$ for methanol and $\varepsilon = 78.54$ for water are considered. COSMO has not been used in gas phase ($\varepsilon = 1$).

The adsorption energies E_{ads} of adsorbate–substrate system are defined as follows: $E_{ads} = E_{sub} + E_{mol} - E_{mol/sub}$. Here $E_{mol/sub}$ is the total energy of adsorbate–substrate system in the equilibrium state; E_{sub} and E_{mol} are the total energy of

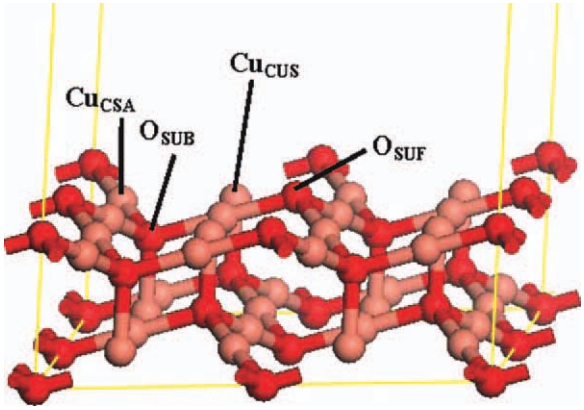

Figure 1. The slab model of $Cu_2O(111)$—2 × 2. Orange balls represent Cu atoms, and red balls represent O atoms.

fixed substrate and free adsorbate alone, respectively. With this definition, positive value of adsorption energy denotes that adsorption is more stable than the corresponding substrate and free adsorbate.

Results and Discussion

The test of calculation method and model

Calculations of CO Molecule and Bulk Cu_2O The obtained values verify the credibility of the selected calculation method: first, the bond length, bond dissociation energy, and stretching frequency of molecular CO calculated from our approach are r(C—O) = 0.1143 nm, E_{BDE} = 1091.24 kJ mol⁻1, and ν_{C-O} = 2128 cm^{-1}, respectively, which are in good agreement with the experimental values of 0.1128 nm,[49] 1076.38 ± 0.67 kJ mol^{-1},[50] and ν_{C-O} = 2138 cm^{-1},[51] respectively, as well as with other similar GGA results.[27] Then, the next test is to predict the lattice constant of bulk Cu_2O. The calculated value for the lattice constant is 0.4430 nm, which is in agreement with the experimental value of 0.4270 nm.[52,53] Such results obtained in these tests make us confident in the research about the mechanism and kinetics of DMC formation on $Cu_2O(111)$ surface.

The Size Effect of Unit Cell on Calculation To investigate the necessary size for supercell, we first compare the adsorption energies and optimized geometries of CO with C-down and CH_3O with O-down adsorbed at Cu_{CUS} site for different supercells. Then, the larger adsorbed systems, such as DMC and CH_3OCO as well as the coadsorption system of CH_3O/OH, CH_3O/CO, CH_3OCO/CH_3O, (CH_3O)(OH)/CH_3OH, $(CH_3O)_2$/CO, and DMC/H_2O adsorbed on $Cu_2O(111)$—[2 × 2] and [2 × 3] surface, have been investigated to further examine the necessary size for supercell. Afterward, the size effects of unit cell on reaction energies and activation barriers, which involves in the reaction of CO insertion to methoxide species and methoxide reaction with carbomethoxide to form DMC on $Cu_2O(111)$—[2 × 2] and [2 × 3] surface, have also been investigated. These discussions about the size effect of unit cell on calculation have also been provided in Supporting Information.

Our calculated results suggest that whether we use [2 × 2] or [2 × 3] supercell, the same results can be obtained. Hence, taking calculation efficiency into consideration, a [2 × 2] supercell is large enough for our researchful system and is used in this study.

Structures and energetics of adsorbed intermediates

To investigate the mechanism and kinetics of DMC formation on $Cu_2O(111)$, we first need to know the individual bonding natures of different species adsorbed, for example, CH_3OH, O, OH, CH_3O, CO, CH_3OCO, and DMC species adsorbed on $Cu_2O(111)$ surface. Four different adsorption sites on $Cu_2O(111)$ surface are considered.

CH_3OH, O, OH, and CH_3O Adsorbed on $Cu_2O(111)$ Surface For the adsorption of CH_3OH, O, OH, and CH_3O adsorbed on $Cu_2O(111)$ surface, they have been reported in our previous studies,[42] in which the Cu_{CUS}, Cu_{CSA}, Cu_{CUS}, and Cu_{CUS} sites are shown to be the most energetically favorable for CH_3OH, O, OH, and CH_3O, respectively, and the corresponding adsorption energies are 89.3, 337.5, 297.9, and 224.9 kJ mol^{-1}, respectively.

In this study, we further calculated the vibrational frequencies of CH_3OH and CH_3O adsorbed on $Cu_2O(111)$ surface, as the experimental results are available for comparison with our calculated results. The calculated frequencies show that bands for CH_3OH are seen at 3046 and 2965 cm^{-1} due to the antisymmetric and symmetric C—H stretching vibrations of molecularly adsorbed CH_3OH, at 1470 cm^{-1} for the deformation of methyl group and at 1330 cm^{-1} for the deformation of OH group. Bands for CH_3O are seen at 2945 and 2879 cm^{-1} due to the antisymmetric and symmetric C—H stretching vibrations of adsorbed methoxide as well as that at 1455 cm^{-1} for the deformation of methyl group. Above calculated frequencies

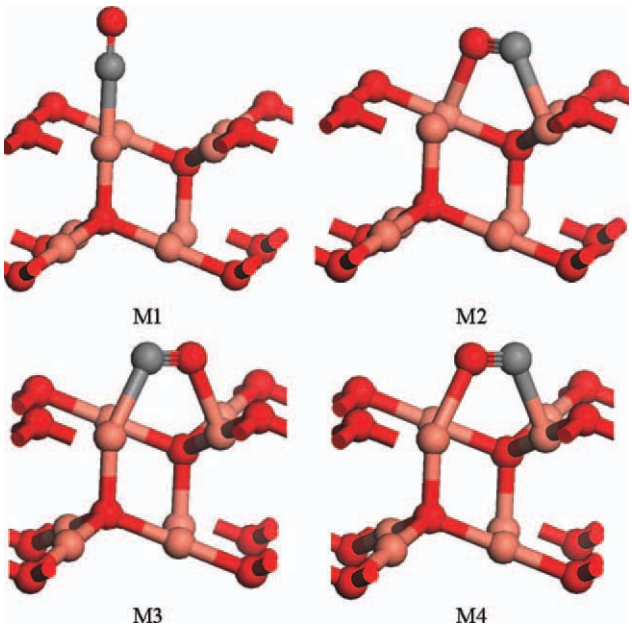

Figure 2. Different adsorption configurations of CO on $Cu_2O(111)$ surface. Grey black balls represent C atoms, and others are the same as in Figure 1.

accord with Bell et al.'s experimental spectrum bands in the oxidative carbonylation of methanol to form DMC on Cu—Y zeolite.[24]

CO/Cu_2O(111) In this study, CO molecule is allowed to approach the Cu_2O(111) surface along two adsorption modes over four distinct sites, one is an end-on mode involving CO perpendicular to the surface (M1), the other is a side-on mode involving CO parallel to the surface (M2–M4). The geometries used in the calculations are presented in Figure 2.

For the end-on mode of CO adsorption, the calculated results of geometry optimization show that the adsorption energies of C-down configuration are much stronger than those of O-down configuration. CO adsorbed with C-down over Cu_{CUS} site is the most stable configuration, the corresponding adsorption energy is 131.1 kJ mol^{-1}, and the corresponding charge transferred from CO to surface is 0.386 *e*. In the optimized structure, the C—O and Cu—C bond lengths are 0.1149 and 0.1835 nm, respectively. The angle of O—C—Cu_{CUS} is 179.9°. The C—O stretching vibrational frequency of CO adsorbed is significantly red-shifted from 2128 cm^{-1} of free CO molecule to 2073 cm^{-1}. For the side-on mode of M2 and M3, when the calculations of geometry optimization are performed to obtain the most stable adsorption configuration, the initial configurations of the side-on M2 and M3 modes are optimized to M1 mode with C-down toward the surface. However, the initial configuration of M4 mode is optimized to M1 mode with O-down toward the surface, the corresponding adsorption energy is 15.1 kJ mol^{-1}, which is typical of a weak physisorption. Above results show that the end-on mode of CO adsorption with C-down over Cu_{CUS} site is the most stable configuration, which is in agreement with the reported studies.[54–56]

CH_3OCO/Cu_2O(111) For the adsorption of CH_3OCO radical on Cu_2O(111) surface, the adsorption models of C-down toward the surface over four different adsorption sites are calculated. These results show that the Cu_{CUS}-bound CH_3OCO interacting with the surface through the C atom of carbonyl group is the most advantageous adsorption model, the corresponding adsorption energy is 204.4 kJ mol^{-1}, and the corresponding charge transferred from CO to surface is 0.014 *e*. Previous work by Drake et al.[12] on Cu—Y zeolite via *in situ* infrared and X-ray absorption near edge structure (*XANES*) has shown that carbonyl groups are associated with Cu cations of the zeolite, which is in agreement with earlier reports of Root and Anderson for Cu—X.[6] In the optimized structure, see Figure 3a, the lengths of O—CH_3, C=O, =C—O, and Cu—C bond are 0.1470, 0.1221, 0.1391, and 0.1934 nm, respectively. The angles of O—C—O and C—O—C are 121.1° and 115.8°, respectively. The calculated bands at 1633 and 1471 cm^{-1} are attributable to the C=O stretching and C—H bending modes of CH_3OCO species associated with Cu_{CUS}, which are in very good agreement with King's experimental spectrum bands at 1630 and 1470 cm^{-1} due to the C=O stretching and C—H bending modes.[8]

DMC/Cu_2O(111) Similarly, for the adsorption of DMC on Cu_2O(111) surface, the adsorption models of O-down toward the surface over four different adsorption sites are also calculated. In all optimized configurations, DMC is found to have a tendency to leave the surface; the adsorption energies are almost near, the configuration in Figure 3b has relatively large adsorption energy of 33.6 kJ mol^{-1}, and the charge transferred from DMC to surface is only 0.022 *e*, which is indicative of a physisorption. In the optimized structure, C=O bond length of DMC is 0.1218 nm, and CO—CH_3 bond lengths are 0.1480 and 0.1471 nm, respectively, as well as two O—CO bond lengths are 0.1374 and 0.1353 nm, respectively.

According to above adsorption energies, the preferential adsorption site for each species involved in the formation mechanism of DMC is obtained, it is evidently found that radical intermediates have a much stronger interaction with the surface than molecules.

Reaction mechanism

After getting the perfected adsorption site for each species involved in DMC formation via oxidative carbonylation of methanol on Cu_2O catalyst, we explore the detailed reaction mechanism by activation barrier calculation in the following section. To determine accurate activation barriers, the transition states for reactions are searched by means of complete linear synchronous transit (LST)/quadratic synchronous transit (QST),[57] starting from reactants and products, the LST method performs a single interpolation to a maximum energy, and the QST method alternates searches for an energy maximum with constrained minimization to refine the transition state to a high degree. This method has been applied to study the adsorption and dissociation of H_2 and CH_3OH on Cu_2O(111) surface in our previous studies.[42,58] In addition, frequency analysis has been used to validate the optimized transition state structures, and TS confirmation is performed on every transition state structure to confirm that they lead to the desired reactants and products.

The reaction mechanism for DMC formation is illustrated in Scheme 1. The individual reaction steps shown have been suggested by the reported experimental work.[3,6,8,16,21,24] The active site is denoted with an asterisk. The notation (X)* is used to represent an active site interacting with species X. In this mechanism, reaction 1 is the molecular adsorption of CH_3OH, then, the molecularly adsorbed $(CH_3OH)^*$ is converted rapidly to $(CH_3O)^*$ and $(OH)^*$ via reaction 2 in the presence of oxygen in the feed. Further, DMC can be formed via two pathways; the first pathway involves reaction 3, in which $(CH_3O)^*$

$$CH_3OH + * \rightarrow (CH_3OH)* \quad (1)$$

$$(CH_3OH)* + O* \rightarrow (CH_3O)*(OH)* \quad (2)$$

Pathway 1

$$(CH_3O)*(OH)* + CH_3OH \rightarrow (CH_3O)_2* + H_2O \quad (3)$$

$$(CH_3O)_2* + CO \rightarrow (DMC)* \quad (4)$$

Pathway 2

$$(CH_3O)* + CO \rightarrow (CH_3OCO)* \quad (5)$$

$$(CH_3OCO)* + (CH_3O)* \rightarrow (DMC)* \quad (6)$$

$$(DMC)* \rightarrow DMC + * \quad (7)$$

Scheme 1. The investigated mechanism for DMC formation by the oxidative carbonylation of methanol.

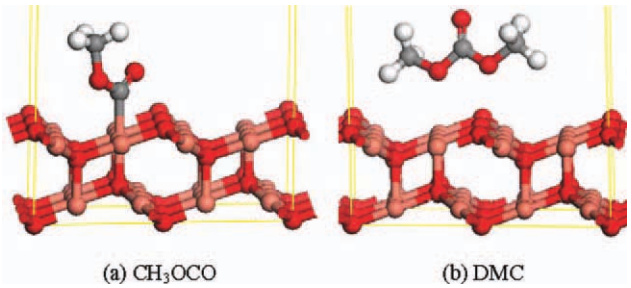

Figure 3. Optimized structure of CH_3OCO and DMC adsorbed on $Cu_2O(111)$ surface. White light balls represent H atoms, and others are the same as in Figures 1 and 2.

and (OH)* produced in reaction 2 react further with CH_3OH to form dimethoxide species $(CH_3O)_2$*; subsequently, CO insertion to $(CH_3O)_2$* produces adsorbed (DMC)* via reaction 4. On the other hand, the second pathway involves reaction 5 of CO insertion to (CH_3O)* forming (CH_3OCO)*, once formed, (CH_3OCO)* reacts rapidly with another CH_3O to form adsorbed (DMC)* via reaction 6; finally, DMC is released into the gas phase via reaction 7. The structures of the reactants, transition states, and products involved in different reactions are shown in Figure 4, and the corresponding imaginary frequency of every transition state is summarized in Table 1.

Table 1. Imaginary frequency of each transition state and the bonds corresponding to relative normal vibration.

Transition state	Imaginary frequency (cm^{-1})	Bonds corresponding to normal vibration[a]
TS1	−101.3	O1—H2—O3
TS2	−451.5	O1—C2; C2—O3; O1—O3
TS3	−335.2	C2—O1
TS4	−347.2	C2—O1

[a] The labels of the atoms (for instance O1—H2—O3, etc.) are presented in Figure 4.

The Formation of CH_3O by CH_3OH in the Presence of Oxygen The work for reactions 1 and 2 in this section has been investigated in our previous studies,[42] the corresponding results

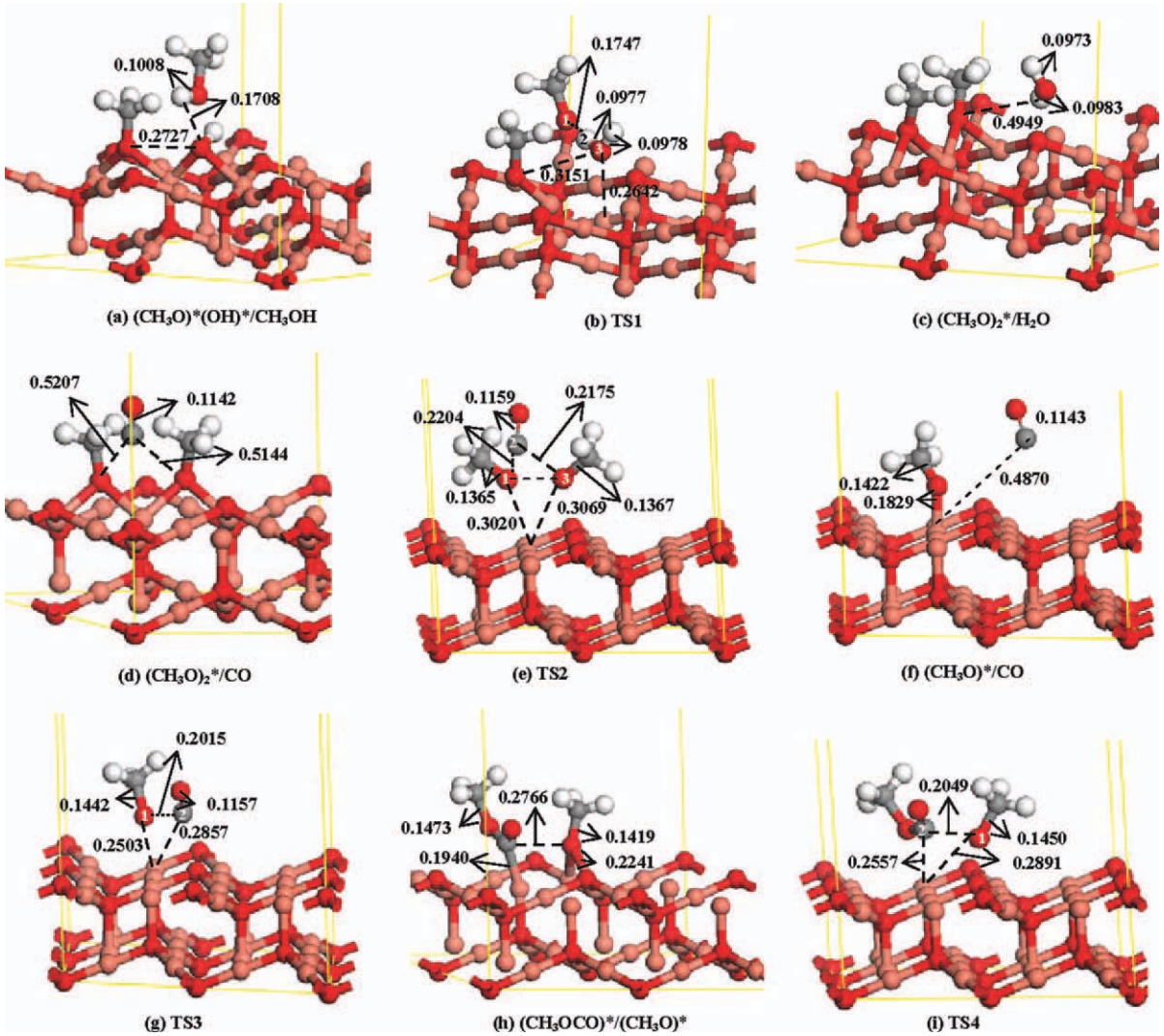

Figure 4. Optimized coadsorbed structures and transition states over $Cu_2O(111)$ surface in different reaction steps (unit: nm). See Figures 1–3 for color coding.

show that the O—H bond-breaking path to form the coadsorption $(CH_3O)^*(OH)^*$ configuration is discovered to be a nonpotential energy-barrier reaction, and this reaction is found to be exothermic by 22.5 kJ mol^{-1}, suggesting that the presence of O_{ad} on $Cu_2O(111)$ surface exhibits a high surface reactivity toward the formation of CH_3O. Therefore, it is reasonable to assume that reaction 2 can rapidly reach equilibrium. The calculated results are in accordance with the early reported experimental observations,[6,8,12,15,16,21,24] which show that when oxygen is present in the feed, the molecularly adsorbed CH_3OH is converted rapidly to CH_3O species.

The Formation of Dimethoxide Species $(CH_3O)^*$ and $(OH)^*$ produced in reaction 2 can react further with CH_3OH to form the dimethoxide species $(CH_3O)_2^*$ and H_2O via reaction 3. Based on the $(CH_3O)^*(OH)^*/CH_3OH$ and $(CH_3O)_2^*/H_2O$ adsorption configuration, as reaction 3, the formation of dimethoxide species is analyzed. The configuration with key geometrical parameters of the $(CH_3O)^*(OH)^*/CH_3OH$ adsorbed over $Cu_2O(111)$ surface is given in Figure 4a. In this configuration, both CH_3O and OH are adsorbed at the Cu_{CUS}—Cu_{CSA} bridge, CH_3OH lies above $Cu_2O(111)$ surface, and the geometrical structure of CH_3OH are closed to that in the gas phase free molecule. The distance between H atom of OH in CH_3OH and O atom of OH adsorbed is 0.1708 nm, the distances between O atom of CH_3O adsorbed and O atom of OH adsorbed is 0.2727 nm. In addition, the Mulliken charge shows that the charges of CH_3O, OH, and CH_3OH are −0.218, −0.326 and 0.039 *e*, respectively. Thus, $(CH_3O)_2^*$ should be formed from gas phase CH_3OH molecule and adsorbed $(CH_3O)^*(OH)^*$ over $Cu_2O(111)$ surface via the Eley–Rideal (E–R) mechanism.

Further, the $(CH_3O)^*(OH)^*/CH_3OH$ configuration goes through a transition state TS1 (see Fig. 4b), which leads to the formation of dimethoxide species and H_2O (see Fig. 4c), this reaction is slightly endothermic by 10.6 kJ mol^{-1} and has an activation barrier of 68.3 kJ mol^{-1} via TS1. In TS1, hydrogen migration from O atom of CH_3OH to O atom of OH adsorbed leads to the formation of additional $(CH_3O)^*$ and H_2O. The O—H distance greatly increased from 0.1008 in CH_3OH to 0.1747 nm, suggesting that the O—H bond in CH_3OH is broken. The distance between H atom of OH in CH_3OH and O atom of OH adsorbed is shortened from 0.1708 to 0.0977 nm, indicating that the O—H bond is formed. In addition, in TS1, the Mulliken charge of CH_3O is −0.259 *e*, the formed H_2O and CH_3O are 0.083 and −0.406 *e*, respectively. In the $(CH_3O)_2^*/H_2O$ configuration (see Fig. 4c), two CH_3O adsorbed at the Cu_{CUS}—Cu_{CSA} bridge with the Mulliken charge of −0.277 and −0.283 *e*, respectively. H_2O, which is formed by the adsorbed OH accepting H atom of OH in CH_3OH, is inclined to keep away from $Cu_2O(111)$ surface with the Mulliken charge of 0.012 *e*. The O—H bond lengths of H_2O are 0.0973 and 0.0983 nm, respectively. The O—H distance between H atom of H_2O and O atom of CH_3O adsorbed is 0.4949 nm.

Insertion of CO to Dimethoxide Species to DMC As literature reported that $(CH_3O)_2^*$ cannot be discerned experimentally because the vibrational spectra of CH_3O group in this species and in $(CH_3O)^*$ are virtually the same. So Bell and coworker[24] thought DMC could be formed involving CO insertion to $(CH_3O)_2^*$ to produce adsorbed DMC. Based on the $(CH_3O)_2^*/CO$ and (DMC)*, the first pathway by which DMC can be formed is studied, which involves CO insertion to $(CH_3O)_2^*$ to produce adsorbed DMC, via reaction 4. For reaction 4, as CH_3O adsorption is stronger than CO adsorption on $Cu_2O(111)$ surface (224.9 *vs.* 131.1 kJ mol^{-1}), CH_3O will occupy the preferred site over CO in the $(CH_3O)_2^*/CO$ configuration. The configuration with key geometrical parameters of $(CH_3O)_2^*/CO$ over $Cu_2O(111)$ surface is given in Figure 4d. Two CH_3O adsorbed at the Cu_{CUS}—Cu_{CSA} bridge completely inhibit the adsorption of CO, which results in the displacement of CO from the surface. Moreover, the Mulliken charges of two adsorbed CH_3O are −0.255 and −0.269 *e*, respectively. CO is only −0.007 *e*, which supports the conclusions of geometrical structure. Further, the calculated results are in excellent agreement with the early experimental observations,[59,60] which showed that the formation of methoxide species bound to Cu cations completely inhibited the adsorption of CO. The C—O bond of CO is 0.1142 nm, which is closed to that (0.1143 nm) in the gas phase CO molecule. The distances between O atom of CH_3O adsorbed and C atom of CO are 0.5207 and 0.5144 nm, respectively. So DMC is formed via the E–R mechanism from gas phase CO and adsorbed $(CH_3O)_2^*$ over $Cu_2O(111)$ surface.

This reaction step is significantly exothermic by 213.5 kJ mol^{-1}. However, the corresponding activation barrier of 308.5 kJ mol^{-1} is very large. The transition state TS2 of this later CO insertion step is shown in Figure 4e. In TS2, two CH_3O leave the surface, and the distances between Cu_{CUS} and O atom of OCH_3 are elongated to 0.3020 and 0.3069 nm to accommodate CO insertion, respectively. The C—O bond of CO is elongated from 0.1142 to 0.1159 nm. The distances of CO with $(CH_3O)_2^*$ decrease from 0.5207 and 0.5144 nm to 0.2204 and 0.2175 nm, respectively. In addition, the Mulliken charge in TS1 show that two CH_3O, respectively, lose 0.028 and 0.050 *e* in comparison with those in $(CH_3O)_2^*/CO$, CO with −0.009 *e* has no obvious change. The overall charge of all adsorbed species in TS1 is −0.455 *e*, which lose 0.076 *e* from $(CH_3O)_2^*/CO$ with −0.531 *e*. In DMC, the charge transferred from DMC to surface is only 0.022 *e*.

Insertion of CO to Methoxide Species For reaction 5, CH_3O still occupies the preferred site over CO in the $(CH_3O)^*/CO$ configuration. The configuration with key geometrical parameters of $(CH_3O)^*/CO$ over $Cu_2O(111)$ surface is given in Figure 4f. We can see that in the $(CH_3O)^*/CO$ configuration, the O—Cu distance of H_3CO—Cu_{CUS} bond is 0.1829 nm, and the distance between Cu_{CUS} and C atom of CO is 0.4870 nm. CO becomes the gas phase CO molecule with the C—O bond length of 0.1143 nm, and the corresponding adsorption energy of CO is only 11.3 kJ mol^{-1} with the charge transferred of only 0.004 *e* from surface to CO, which is far less than the single adsorption of CO over $Cu_2O(111)$ surface with the adsorption energy of 131.1 kJ mol^{-1}, and corresponding charge transferred from CO to surface is 0.386 *e*. However, the adsorption energy of CH_3O is 226.4 kJ mol^{-1} with the charge of −0.256 *e*, which is in agreement with the single adsorption of CH_3O on $Cu_2O(111)$ surface with the adsorption energy of 224.9 kJ mol^{-1} with the

charge of −0.244 *e*, suggesting that the adsorption of methoxide results in complete displacement of the CO adsorbed over Cu_{CUS}, in which CO is more weakly bound. Our results still accord with the early experimental observations,[59,60] which showed that the formation of methoxide species bound to Cu cations completely inhibited the adsorption of CO. Thus, (CH_3OCO)* should be formed from gas phase CO and adsorbed (CH_3O)* over $Cu_2O(111)$ surface via the E–R mechanism. In addition, the calculated C—O stretching frequency of CO in the (CH_3O)*/CO system is significantly red-shifted from 2128 cm^{-1} of free CO molecule to 2107 cm^{-1}. The frequencies at 2932 and 2868 cm^{-1} belong to the antisymmetric and symmetric C—H stretching vibrations of adsorbed methoxide, that at 1448 cm^{-1} for the deformation of methyl group.

Based on (CH_3O)*/CO and (CH_3OCO)* adsorption, as reaction 5, CO insertion to methoxide species forming monomethyl carbonate species is calculated. This reaction is found to be exothermic by 54.0 kJ mol^{-1} and has an activation barrier of 161.9 kJ mol^{-1} via a transition state TS3 (see Fig. 4g). In TS3, CO inserts into the Cu_{CUS}—OCH_3 bond with the Cu_{CUS}—O distance of 0.2503 nm and the C—O distance of 0.1442 nm. The Cu_{CUS}—O distance greatly increased from 0.1829 to 0.2503 nm to accommodate the insertion of CO. The C—O bond of CO is elongated to 0.1157 nm with the Mulliken charge of −0.061 *e*, when the C atom of CO approaches Cu_{CUS} site, the distance between Cu_{CUS} and C atom of CO decreases from 0.4870 to 0.2857 nm. Besides it, the charge transferred from surface to CH_3O in TS3 is 0.317 *e*. In (CH_3OCO)*, the Mulliken charge of CH_3OCO adsorbed is 0.014 *e*.

Methoxide Reaction with Carbomethoxide to DMC Once CH_3OCO is formed, (CH_3OCO)* can react further with another (CH_3O)* to form adsorbed DMC via reaction 6. An early experimental research by Romano et al.[3] has suggested that CO can interact with copper methoxide to form carbomethoxide, and the carbomethoxide reacts further with another copper methoxide to form DMC. Therefore, based on the (CH_3OCO)*/(CH_3O)* coadsorption and (DMC)*, reaction 6 is studied. The (CH_3OCO)*/(CH_3O)* configuration with key geometrical parameters is given in Figure 4h, we can see that CH_3OCO adsorbed over Cu_{CUS} site with a C—Cu_{CUS} distance of 0.1940 nm and a C=O distance of 0.1223 nm. The Mulliken charge of CH_3OCO is 0.042 *e*. CH_3O adsorbed at Cu_{CSA}—Cu_{CSA} bridge site with Cu_{CSA}—O distances of 0.2173 and 0.2241 nm, respectively. The Mulliken charge of CH_3O is −0.263 *e*. The C—O distance of two adsorbed species is 0.2766 nm. Above results indicate that DMC can be formed via the Langmuir–Hinshelwood mechanism from the coadsorbed (CH_3OCO)* and (CH_3O)* on $Cu_2O(111)$ surface.

This reaction step is found to be exothermic largely by 148.9 kJ mol^{-1} and has an activation barrier of 98.8 kJ mol^{-1} via a transition state TS4 (see Fig. 4i). In TS4, both CH_3OCO and CH_3O leave the surface with the C—Cu_{CUS} and O—Cu_{CUS} distance of 0.2557 and 0.2891 nm, respectively. The C=O bond length of 0.1207 nm is close to that of 0.1218 nm in DMC adsorbed, as shown in Figure 2f. Moreover, CH_3O obtains 0.015 *e*, CH_3OCO losses 0.045 *e* in comparison with those in (CH_3OCO)*/(CH_3O)* configuration. The overall charge of all adsorbed species in TS1 is −0.191 *e*, which lose 0.030 *e* in comparison with $(CH_3OCO)_2$*/(CH_3O)*. With CH_3OCO approaching to CH_3O, the distance between radical C of CH_3OCO and O of CH_3O decreases from 0.2766 to 0.2049 nm, which lead to the adsorbed DMC with the Mulliken charge of 0.022 *e*. Above calculated results suggest that reaction 6 is a much favored process to form DMC on $Cu_2O(111)$ surface.

Finally, DMC adsorbed is released into the gas phase via reaction 7, this reaction is endothermic by 33.6 kJ mol^{-1}, which can be easily compensated by the exothermic reaction of DMC formation about 148.9 and 213.5 kJ mol^{-1}.

Brief Summary Figure 5 presents the potential energy profile with the relative energy values of each elementary reaction in

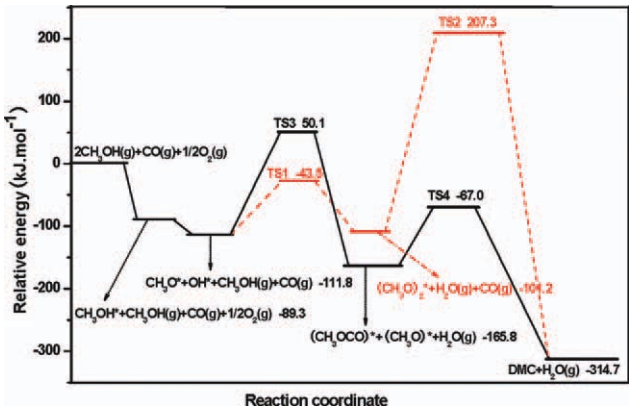

Figure 5. The energy profiles with the energy values for the whole DMC formation in different pathways without solvent. [Color figure can be viewed in the online issue, which is available at wileyonlinelibrary.com.]

the mechanism of DMC formation on $Cu_2O(111)$ surface. For the first pathway of DMC formation involving in reactions 3 and 4, as shown in Figure 5 using a red line, the corresponding activation barriers of reactions 3 and 4 are 68.3 and 308.5 kJ mol^{-1}, respectively, so reaction 4 is thought to be the rate-determining step for the first pathway of DMC formation. For the second pathway of DMC formation including reactions 5 and 6, as shown in Figure 5 using a black line, the corresponding activation barriers of reactions 5 and 6 are 161.9 and 98.8 kJ mol^{-1}, respectively, so reaction 5 is thought to be the rate-determining step for the second pathway of DMC formation.

Then, when activation barriers of the rate-determining step (308.5 *vs.* 161.9 kJ mol^{-1}) are compared in these two pathways, it can be concluded that the first pathway of DMC formation involving in reactions 3 and 4 is not in competition with the second pathway of DMC formation including reactions 5 and 6. Therefore, we think the main reaction pathway of DMC formation is made up of reactions 1, 2, and 5–7, as shown in Figure 5 using a black line. Above results answer the first question proposed in the introduction, the second pathway mainly contribute to the formation of DMC. Methanol first adsorbs in the presence of oxygen to form coadsorbed methoxide and hydroxyl species on $Cu_2O(111)$ surface (reactions 1 and 2). DMC can form by CO addition to methoxide to produce monomethyl carbonate species (reaction 5), which then react with additional methoxide to form DMC directly (reaction

6), finally, DMC is released into the gas phase via reaction 7. Our results provide a theoretical guidance for the reported experimental facts.[3,6,8,12,13,21] In addition, it is noted that when reactions 5 and 6 for DMC formation occur as a central component of the main pathway, a very small quantity of DMC may be also formed by reactions 3 and 4, which need to overcome a very large activation barrier.

Further, as a periodic slab model is used to investigate the mechanism of DMC formation in this study, we compare the reaction energies and activation barriers of the rate-determining step for two pathways of DMC formation in this work with the values reported by the single Cu^+ atom supported on Y zeolite cluster model of Bell et al.[38] to understand the difference between periodic model and cluster model. The studies by Bell et al. showed that insertion of CO to methoxide species has an activation barrier of 55.2 (161.9) kJ mol^{-1}, and exothermic by 300.8 (54.0) kJ mol^{-1}. Insertion of CO to dimethoxide species to DMC has an activation barrier of 62.8 (308.5) kJ mol^{-1}, and exothermic by 284.1 (213.5) kJ mol^{-1}. Our results are displayed in the parentheses. We can see that the difference between periodic model and single atom cluster model is likely because of cluster size effects where only single metallic atom is used. However, the trend obtained by Bell and coworker,[38] the activation barrier of insertion of CO to dimethoxide species to DMC is larger than that of insertion of CO to methoxide species, is in agreement with our current calculations. In addition, the geometrical configurations also show that the adsorption behavior of coadsorbed systems over single Cu^+ ions supported on Y zeolite certainly differs from that over Cu^+ ions in Cu_2O due to the different chemical environment. Therefore, we think that although the single atom cluster model can be used to obtain useful information about DMC mechanism, to a certain extent, the periodic slab model can rather well model and reflect a specific crystal plane of the catalyst under the realistic conditions of DMC formation.

The effect of solvent on CO insertion to methoxide species

Above kinetics results of elementary steps have shown that CO insertion to methoxide species is the rate-determining step of the main reaction pathway for DMC formation in gas phase, which provide a theoretical guidance for the reported experimental facts. So solvent effects (such as, methanol and water) on the reaction of CO insertion to methoxide species involving in the structural parameters, adsorption energies, reaction energies, and activation barriers have been assessed by using COSMO model in this section.

The Effect of Solvent on (CH_3O)*/CO Structure All the geometries are optimized again in solvent and the corresponding key geometrical parameters of the optimized (CH_3O)*/CO structure are given in Table 2. In the (CH_3O)*/CO configuration, the C—O bond length of CO is elongated from 0.1143 nm in gas phase to 0.1157 nm in methanol and 0.1160 nm in water, respectively, which show that solvent effect can reduce the strength of C—O bond and make the C—O bond activation. The elongation of C—O bond leads to the red-shift of C—O stretching vibrational frequency. CO inserts into the Cu—OCH_3 bond with a Cu_{CUS}—OCH_3 distance of 0.1898 nm in methanol and 0.1902 nm in water. Compared to Cu_{CUS}—OCH_3 distance of 0.1829 nm in gas phase, solvent effects can make the Cu—OCH_3 distance increase to accommodate the insertion of CO much easier. With the C atom of CO approaching to Cu_{CUS} site, the distance between Cu_{CUS} and C atom of CO decreases to 0.4119 nm in methanol and 0.4094 nm in water. Above geometrical parameters show that although the differences between the calculated geometrical parameters in gas phase and those in solvents do not appear to be large, we can obtain a preliminary understanding of solvent effects on the CO insertion to methoxide, which suggest that solvent effects can improve the ability of CO insertion to methoxide over $Cu_2O(111)$ surface.

Table 2. Calculated geometrical parameters of the (CH_3O)*/CO adsorption configuration over $Cu_2O(111)$ surface in different solvents.

Parameters[a]	Gas phase	Methanol	Water
C—O (nm)	0.1143	0.1157	0.1160
ν_{C-O} (cm^{-1})	2107	1960	1920
H_3CO—Cu_{CUS} (nm)	0.1829	0.1898	0.1902
O—CH_3 (nm)	0.1422	0.1403	0.1405
OC—Cu_{CUS} (nm)	0.4870	0.4119	0.4094
α (°)	124.6	123.3	123.3

[a] α stands for the angle between the adsorbed site and CH_3O after adsorption.

The Effect of Solvent on Adsorption Energies COSMO model has been applied to calculate the adsorption energies of the (CH_3O)*/CO configuration, transition state TS3, and CH_3OCO over $Cu_2O(111)$ surface in methanol and water solvents, the results are listed in Table 3. We can see that solvent destabilizes the (CH_3O)*/CO adsorption configuration, the adsorption energy of (CH_3O)*/CO decreases from 244.8 kJ mol^{-1} in gas phase to 189.8 kJ mol^{-1} in methanol and 188.9 kJ mol^{-1} in water, which may increase the ability of CO insertion to methoxide. Moreover, the overall charges transferred from surface to CO and CH_3O are 0.260, 0.241, and 0.240 *e* in gas phase, methanol, and water, respectively. However, the adsorption energy of transition state TS3 increases from 82.9 kJ mol^{-1} in gas phase to 119.6 kJ mol^{-1} in methanol and 125.0 kJ mol^{-1} in water, which suggests solvent can well stabilize the transition states TS3. Similarly, the Mulliken charge in TS3 also show that the overall charges transferred from surface to adsorbed species are 0.378, 0.396, and 0.401 *e* in gas phase, methanol, and water, respectively, which is in agreement with the adsorption energy. The adsorption energies of CH_3OCO increase slightly with 299.0 kJ mol^{-1} in methanol and 301.1 kJ mol^{-1} in

Table 3. Calculated adsorption energies of (CH_3O)*/CO, transition state TS3 and (CH_3OCO)* adsorption over $Cu_2O(111)$ surface in different solvents.

	E_{ads} (kJ mol^{-1})		
Adsorbed species	Gas phase	Methanol	Water
(CH_3O)*/CO	244.8	189.8	188.9
TS3	82.9	119.6	125.0
(CH_3OCO)*	298.8	299.0	301.1

water when these results are in comparison with that 298.8 kJ mol^{-1} in gas phase. Nevertheless, the Mulliken charge in CH_3OCO adsorbed suggest that solvent can change the direction of charge transfer, in gas phase, the charge transfers from CH_3OCO to surface about 0.014 *e*. However, in methanol and water, the charge transfers from surface to CH_3OCO about 0.036 and 0.037 *e* in methanol and water, respectively. Above calculated results show that solvent plays a fundamental role in stabilization of the transition structures, which may reduce the activation barrier of CO insertion to methoxide species.

The Effect of Solvent on Reaction Energies and Activation Barriers To confirm above results deduced by adsorption energy, the reaction energies and activation barriers of insertion reaction in solvents are discussed, and the corresponding results are presented in Figure 6. When the reaction energies

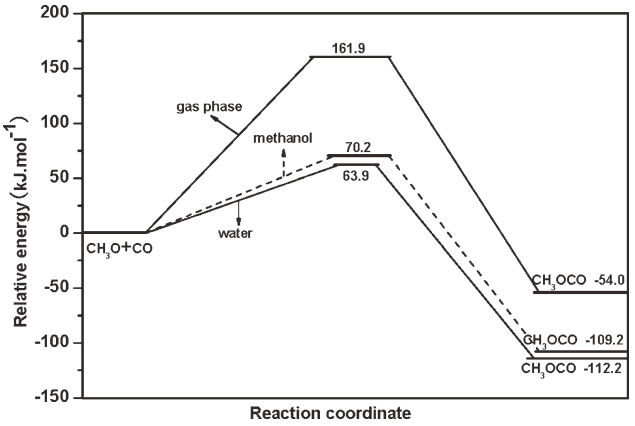

Figure 6. The energy profiles with the energy values involving in the reaction of CO insertion to methoxide species in different solvents.

and activation barriers in gas phase are compared with those after COSMO treatment, it can be found that the effect associated with solvent is very sensitive to the reaction energies and activation barriers. As shown in Figure 6, it can be clearly seen that CO insertion to methoxide species over Cu_2O(111) in methanol need to overcome an activation barrier of 70.2 kJ mol^{-1}, and this reaction is exothermic by 109.2 kJ mol^{-1}. In water, the activation barrier is calculated to be 63.9 kJ mol^{-1}, this reaction is strongly exothermic by 112.2 kJ mol^{-1}. The activation barrier 63.9 kJ mol^{-1} obtained in water solvent is in excellent agreement with the experimental value 61.9 kJ mol^{-1}.[24,38]

Brief Summary Compared to CO insertion to methoxide species over Cu_2O(111) surface in solvent and that in gas phase, as shown in Figure 6, the reaction energies and activation barriers show that solvent can well reduce the activation barrier of CO insertion to methoxide species, and make the insertion reaction more exothermic, indicating that solvent is in favor of insertion reaction both thermodynamically and kinetically. Above results answer the second question proposed in the introduction, the role of solvent environment in the liquid-phase slurry can modify the reaction energies and activation barriers of CO insertion to methoxide in a significant way. These results emphasize that the reaction of CO insertion to methoxide mediated by solvent is a favored process, which means that the performance of DMC formation on Cu_2O catalyst in a liquid-phase slurry is much easier than that in gas phase.

Conclusions

In this study, we use the DFT method to fully investigate the reaction energies and activation barriers for the elementary steps involving in DMC formation via oxidative carbonylation of methanol on Cu_2O (111) surface. Our results show that the formation of methoxide group bound to Cu_{CUS} site in (CH_3O)*/CO system completely inhibit the adsorption of CO, reducing the adsorption energy of CO, and making the C—O stretching vibration red-shift; these calculated results are also in excellent agreement with experimental observations. Then, the kinetics results show that CO insertion to methoxide species to produce monomethyl carbonate species and monomethyl carbonate species reacting with methoxide to form DMC is the main reaction pathway of DMC formation, and CO insertion to dimethoxide species to produce DMC is not competitive. Finally, solvent effects by using COSMO model are considered to investigate CO insertion to methoxide species, the reaction energies and activation barriers show that solvent effects can well reduce the reaction energies and activation barriers of insertion reaction, and make insertion reaction much favorable both thermodynamically and kinetically, which means that CO insertion to methoxide species mediated by solvent is a favored process.

Acknowledgments

The authors thank for anonymous reviewers for their helpful suggestions on the quality improvement of this article.

Keywords: dimethyl carbonate · Cu_2O · mechanism · solvent effect · density functional theory

How to cite this article: R. Zhang, L. Song, B. Wang, Z. Li, *J. Comput. Chem.* **2012**, *33,* 1101–1110. DOI: 10.1002/jcc.22939

Additional Supporting Information may be found in the online version of this article.

[1] Y. Ono, *Appl. Catal. A: Gen.* **1997**, *155,* 133.
[2] S. A. Anderson, S. Manthata, T. W. Root, *Appl. Catal. A: Gen.* **2005**, *280,* 117.
[3] U. Romano, R. Tesel, M. M. Mauri, P. Rebora, *Ind. Eng. Chem. Prod. Res. Dev.* **1980**, *19,* 396.
[4] K. Tomishige, T. Sakaihori, S. Sakai, K. Fujimoto, *Appl. Catal. A: Gen.* **1999**, *181,* 95.
[5] S. T. King, M. E. Jones, M. M. Olken, U.S. Patent 539,1803, **1995**.
[6] S. A. Anderson, T. W. Root, *J. Mol. Catal. A: Chem.* **2004**, *220,* 247.
[7] Y. J. Wang, X. Q. Zhao, B. G. Yuan, B. C. Zhang, J. S. Cong, *Appl. Catal. A: Gen.* **1998**, *171,* 255.
[8] S. T. King, *J. Catal.* **1996**, *161,* 530.
[9] U. Romano, *Chim. Ind.* **1993**, *75,* 303.
[10] X. B. Ma, R. Z. Zhao, G. H. Xu, F. He, H. F. Chen, *Catal. Today* **1996**, *30,* 201.
[11] Z. Li, K. C. Xie, R. C. T. Slade, *Appl. Catal. A: Gen.* **2001**, *205,* 85.
[12] I. J. Drake, Y. H. Zhang, D. Briggs, B. Lim, T. Chau, A. T. Bell, *J. Phys. Chem. B* **2006**, *110,* 11654.

[13] Y. H. Zhang, I. J. Drake, D. N. Briggs, A. T. Bell, *J. Catal.* **2006**, *244,* 219.
[14] Y. H. Zhang, I. J. Drake, A. T. Bell, *Chem. Mater.* **2006**, *18,* 2347.
[15] Y. H. Zhang, D. N. Briggs, E. de Smit, A. T. Bell, *J. Catal.* **2007**, *251,* 443.
[16] S. A. Anderson, T. W. Root, *J. Catal.* **2003**, *217,* 396.
[17] Z. Li, F. H. Meng, J. Ren, H. Y. Zheng, K. C. Xie, *Chin. J. Catal.* **2008**, *29,* 643.
[18] J. Ren, S. S. Liu, Z. Li, X. L. Lu, K. C. Xie, *Appl. Catal. A: Gen.* **2009**, *366,* 93.
[19] M. A. Pacheco, C. L. Marshall, *Energy Fuels* **1997**, *11,* 2.
[20] Y. J. Wang, R. X. Jiang, X. Q. Zhao, S. F. Wang, *J. Nat. Gas Chem.* **2000**, *9,* 205.
[21] S. T. King, *Catal. Today* **1997**, *33,* 173.
[22] Z. Li, C. M. Wen, R. Y. Wang, H. Y. Zheng, K. C. Xie, *Chem. J. Chin. Univ.* **2009**, *30,* 2024.
[23] Z. Li, C. M. Wen, R. Y. Wang, H. Y. Zheng, K. C. Xie, *Chem. J. Chin. Univ.* **2010**, *31,* 145.
[24] Y. H. Zhang, A. T. Bell, *J. Catal.* **2008**, *255,* 153.
[25] Z. J. Zuo, W. Huang, P. D. Han, Z. H. Li, *J. Mol. Model.* **2009**, *15,* 1079.
[26] Z. J. Zuo, W. Huang, P. D. Han, Z. H. Li, *Acta Phys. Chim. Sin.* **2009**, *25,* 2507.
[27] Z. J. Zuo, W. Huang, P. D. Han, Z. H. Li, *Appl. Surf. Sci.* **2010**, *256,* 2357.
[28] E. F. de Lima, J. W. M. Carneiro, C. Fenollar-Ferrer, S. Miertus, S. Zinoviev, N. C. Om Tapanes, D. A. G. Aranda, *Fuel* **2010**, *89,* 685.
[29] N. E. Hall, B. J. Smith, *J. Phys. Chem. A* **1998**, *102,* 3985.
[30] N. E. Hall, B. J. Smith, *J. Phys. Chem. A* **1998**, *102,* 4930.
[31] X. L. Luo, D. Y. Tang, M. Li, *Acta Phys. Chim. Sin.* **2004**, *20,* 1404.
[32] D. Jacquemin, J. Preat, E. A. Perpète, *Chem. Phys. Lett.* **2005**, *410,* 254.
[33] N. Sanna, G. Chillemi, A. Grandi, S. Castelli, A. Desideri, V. Barone, *J. Am. Chem. Soc.* **2005**, *127,* 15429.
[34] J. Tomasi, B. Mennucci, R. Cammi, *Chem. Rev.* **2005**, *105,* 2999.
[35] D. Jacquemin, E. A. Perpete, G. Scalmani, M. J. Frisch, I. Ciofini, C. Adamo, *Chem. Phys. Lett.* **2006**, *421,* 272.
[36] J. Sebek, Z. Kejik, P. Bour, *J. Phys. Chem. A* **2006**, *110,* 4702.
[37] C. Dykstra, G. Frenking, K. Kim, G. Scuseria, Theory and Applications of Computational Chemistry; Elsevier: Amsterdam, **2005**.
[38] X. B. Zheng, A. T. Bell, *J. Phys. Chem. C* **2008**, *112,* 5043.
[39] H. Burghgraef, A. P. J. Jansen, R. A. van Santen, *Surf. Sci.* **1995**, *324,* 345.
[40] M. M. Islam, B. Diawara, V. Maurice, P. Marcus, *J. Mol. Struct. (Theochem.)* **2009**, *903,* 41.
[41] K. H. Schulz, D. F. Cox, *Phys. Rev. B* **1991**, *43,* 1610.
[42] R. G. Zhang, H. Y. Liu, L. X. Ling, Z. Li, B. J. Wang, *Appl. Surf. Sci.* **2011**, *257,* 4232.
[43] B. Delley, *J. Chem. Phys.* **1990**, *92,* 508.
[44] B. Delley, *J. Chem. Phys.* **2000**, *113,* 7756.
[45] A. Klamt, G. Schrmann, *J. Chem. Soc. Perkin Trans.* **1993**, *2,* 799.
[46] A. Klamt, V. Jonas, T. Bürger, J. C. W. Lohrenz, *J. Phys. Chem. A* **1998**, *102,* 5074.
[47] T. Todorova, B. Delley, *Mol Simul.* **2008**, *34,* 1013.
[48] A. V. Gavrilenko, T. D. Matos, C. E. Bonner, S. S. Sun, C. Zhang, V. I. Gavrilenko, *J. Phys. Chem. C* **2008**, *112,* 7908.
[49] J. X. Shao, X. L. Cheng, X. D. Yang, F. P. Zhang, S. H. Ge, *J. At. Mol. Phys.* **2006**, *23,* 80.
[50] Y. R. Luo, Handbook of Bond Dissociation Energies in Organic Compounds; Science Press: Beijing, **2005**; p. 209.
[51] B. Z. Sun, W. K. Chen, J. D. Zheng, C. H. Lu, *Appl. Surf. Sci.* **2008**, *255,* 3141.
[52] R. Restori, D. Schwarzenbach, *Acta Crystallogr. B* **1986**, *42,* 201.
[53] M. A. Nygren, L. G. M. Pettersson, *J. Phys. Chem.* **1996**, *100,* 1874.
[54] M. Casarin, C. Maccato, A. Vittadini, *Chem. Phys. Lett.* **1997**, *280,* 53.
[55] B. Thomas, P. Gianfranco, *Surf. Sci.* **2007**, *373,* 21.
[56] M. Casarin, A. Vittadini, *Surf. Sci.* **1997**, *387,* 1079.
[57] T. A. Halgren, W. N. Lipscomb, *Chem. Phys. Lett.* **1977**, *49,* 225.
[58] R. G. Zhang, B. J. Wang, L. X. Ling, H. Y. Liu, W. Huang, *Appl. Surf. Sci.* **2010**, *257,* 1175.
[59] A. Zecchina, S. Bordiga, M. Salvalaggio, G. Spoto, D. Scarano, C. Lamberti, *J. Catal.* **1998**, *173,* 540.
[60] R. Kumashiro, Y. Kuroda, M. Nagao, *J. Phys. Chem. B* **1999**, *103,* 89.

Received: 20 May 2011
Revised: 2 January 2012
Accepted: 3 January 2012, and final revision January 3, 2012
Published online on 17 February 2012